





Transforming pure and mixed states using an NMR quantum homogenizer

Maria Violaris ^{1,*},† Gaurav Bhole ^{1,*}, Jonathan A. Jones ¹, Vlatko Vedral^{1,2} and Chiara Marletto¹

¹Clarendon Laboratory, University of Oxford, Parks Road, Oxford OX1 3PU, United Kingdom

²Centre for Quantum Technologies, National University of Singapore, 3 Science Drive 2, Singapore 117543

 (Received 9 September 2020; revised 19 January 2021; accepted 25 January 2021; published 11 February 2021)

The universal quantum homogenizer can transform a qubit from any state to any other state with arbitrary accuracy, using only unitary transformations to perform this task. Here we present an implementation of a finite quantum homogenizer using nuclear magnetic resonance (NMR), with a four-qubit system. We compare the homogenization of a mixed state to a pure state and the reverse process. After accounting for the effects of decoherence in the system, we find the experimental results to be consistent with the theoretical symmetry in how the qubit states evolve in the two cases. We analyze the implications of this symmetry by interpreting the homogenizer as a physical implementation of pure state preparation and information scrambling.

DOI: [10.1103/PhysRevA.103.022414](https://doi.org/10.1103/PhysRevA.103.022414)

I. INTRODUCTION

The quantum homogenizer can transform a qubit initialized in any state, whether pure or mixed, arbitrarily close to any other state. It was originally proposed as a theoretical model for analyzing many-body entanglement within unitary thermalization, with an additional possible application as a quantum safe [1,2]. More generally, it can be used to implement processes such as quantum information scrambling and pure state preparation using only unitary interactions. In this work, we present a nuclear magnetic resonance (NMR) implementation of the quantum homogenizer, using a system of four qubits. We compare the limiting cases of transforming a qubit from a mixed to a pure state and the reverse process and explain how the entropy changes in quantum homogenization are consistent with unitary quantum theory.

The quantum homogenizer is a machine consisting of N identical *reservoir* qubits. These each interact, one by one, with the *system* qubit (the qubit whose state is to be transformed) via a unitary *partial swap*:

$$U = \cos \eta \mathbb{1} + i \sin \eta S. \quad (1)$$

The partial swap is a combination of the identity $\mathbb{1}$ (which does nothing to the two input qubits) and SWAP operation S (which swaps the states of the two input qubits), weighted by the coupling strength parameter η .

It has been shown [1] that if the system qubit interacts with N reservoir qubits via the partial swap, then as $N \rightarrow \infty$, the system qubit state converges to the original state of the reservoir qubits, for *any* coupling strength $\eta \neq 0$. Furthermore, all of the reservoir qubits after the interaction are within some distance d of their original state, which can be made arbitrarily small as coupling strength $\eta \rightarrow 0$. The limit of a perfect homogenization is achieved asymptotically, as N tends

to infinity, with an infinitesimal η . In that limit, any system qubit ρ is sent to the reservoir qubit state ξ , with all the reservoir qubits remaining unchanged:

$$U_N \dots U_1(\rho \otimes \xi^{\otimes N})U_1^\dagger \dots U_N^\dagger \approx \xi^{\otimes N+1}, \quad (2)$$

where $U_k := U \otimes (\otimes_{j \neq k} \mathbb{1}_j)$ denotes the interaction between the system qubit and the k^{th} reservoir qubit. As already remarked in [1], this is not in contrast with the no-cloning theorem, because the homogenizer realizes an approximate, not exact, copying of the quantum state ξ .

The information about the original system qubit's state is seemingly erased, despite all the interactions being unitary and thus information preserving. The information has actually become stored in the infinitesimal entanglement between infinitely many reservoir qubits, which sums to a finite value [1]. This means the homogenizer can be considered as a unitary implementation of an eraser, in the limit of infinitely many qubits.

Erasure began its critical role in fundamental physics with Landauer's principle, used by Bennett to solve the Maxwell's Demon paradox [3]. Since the logical reset process is key for classical information processing, the limits of erasure are likely to constrain practical devices in the near future [4]. While commercial processors are several orders of magnitude away from the fundamental limits on erasure, experiments are beginning to reach the required sensitivity [5–7]. However, the physical implications of information erasure remain controversial [8,9]. There are various proposals for the true constraints on erasure when performed by a physical machine [10–12]. Experimental implementations of systems that perform erasure arbitrarily well through unitary interactions, such as the quantum homogenizer, could enable fundamental insights into the limits of information erasure within quantum theory.

In general, the homogenizer performs quantum information scrambling, where a local quantum state becomes distributed in many-body entanglement and correlations with other qubits [13]. Scrambling is a specific type of decoher-

*These authors contributed equally to this work.

†maria.violaris@magd.ox.ac.uk

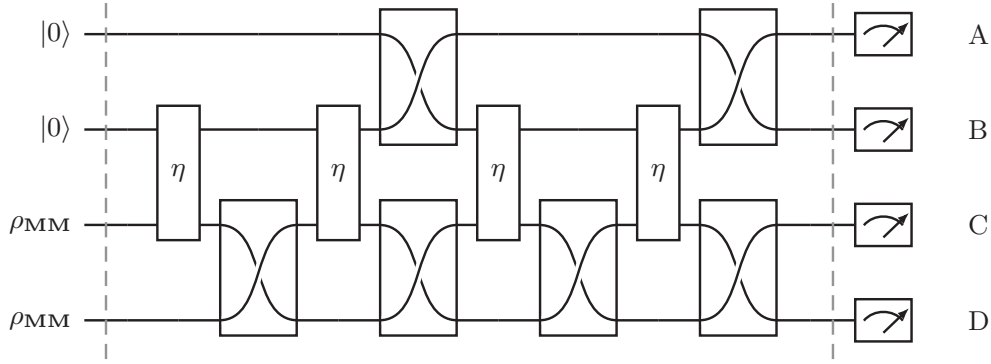


FIG. 1. A quantum homogenizer with two system qubits and two reservoir qubits designed to operate on a linear chain system where two qubit gates are possible only between adjacent qubits. Homogenization is achieved using the partial swap gates, labeled as η , which connect the two middle qubits, while full SWAP gates are used to rotate the system and reservoir registers to bring other qubit pairs into contact. The dashed lines divide the simulation into its initialization, homogenization and readout phases. Qubit labels on the right hand side correspond to spins in the NMR spin system in Fig. 2.

ence, which has been incorporated into unitary models for thermalization in quantum thermodynamics [14,15]. More exotically, it has also been proposed as a model for the information processing of a black hole [16,17]. Additionally, it provides a mechanism for cryptography: a scrambled qubit’s original quantum state can only be recovered with the classical knowledge of its past interactions, securing the quantum information [1]. Homogenization through scrambling forms a many-body entangled system, notoriously difficult to probe analytically due to the exponential complexity when entangling additional qubits. This heightens the need for experimental implementations of information scrambling systems.

As a special case of homogenization, the homogenizer can be used to transform a qubit from any state to a pure state, to arbitrary accuracy. Pure state preparation has crucial practical implications for the resources required for quantum computation. The achievement of fault-tolerant quantum computation requires error correction, which has been proven to require a constant supply of pure ancillary qubits [18]. Hence, quantum models that can produce pure states through unitary dynamics are of particular interest for quantum technology.

II. EXPERIMENTAL SIMULATION

The quantum circuit used in our simulation is shown in Fig. 1. This circuit simulates the homogenization between two system qubits, initially in the pure state $|0\rangle$, and two reservoir qubits, initially in the maximally mixed state ρ_{MM} , and has been designed for implementation on a linear chain where two-qubit gates are only available between adjacent qubits. Partial swap gates are implemented between qubits B and C, while full SWAPs are used to rotate the system and reservoir registers, permitting indirect contact between any pair of qubits.

As we are using an NMR implementation for our simulation we do not have access to qubits in pure states, but instead use ensemble qubits in *pseudopure* states [19,20], or *effective-pure* states [21,22]. As the pure component of these mixed states evolves in precisely the same way under unitary transformations as the desired pure state, and the maximally

mixed component is not detectable in NMR experiments, pseudo-pure states behave exactly like the corresponding pure states except that the signal intensity is reduced. Note, however, that preparation of a pure initial NMR state is possible in special cases [23], and that NMR implementations run using such states produce identical results to those with pseudo-pure states except for the increased signal size [24,25].

The four qubit state before the final readout stage depends on the coupling strength η , but in general is an entangled state. However the final readout stage involves an implicit partial trace over the other three qubits, leaving four separate single-qubit states, all of which lie along the z axes of the respective Bloch spheres, permitting the state to be fully characterized by measurements in the computational basis. We can write for each qubit

$$\rho = \frac{\mathbb{1}}{2} + f(\eta) \times \frac{\sigma_z}{2}, \tag{3}$$

where

$$f = \text{tr}(\rho\sigma_z) \tag{4}$$

lies in the range ± 1 , and corresponds to the difference between the probabilities of finding $|0\rangle$ or $|1\rangle$ when measuring a qubit in the computational basis. For our circuit, f is confined to lie between 0 and 1, and in particular, we find for the individual qubits the forms

$$f_B = \cos^4(\eta) \tag{5}$$

and $f_C = 1 - f_B$, so that f_B falls smoothly from 1 to 0, while f_C rises in the opposite way. Similarly,

$$f_A = 4 \cos^2(\eta) - 9 \cos^4(\eta) + 8 \cos^6(\eta) - 2 \cos^8(\eta) \tag{6}$$

also falls from 1 to 0, but following a more complex pattern, with $f_D = 1 - f_A$ once again rising in the opposite way.

As the coupling strength η is increased the homogenization becomes more effective, and for circuits with the same number of system and reservoir qubits the states are completely interchanged in the limiting case $\eta = \pi/2$. This symmetry permits the roles of the system and reservoir qubits to be interchanged, and so this homogenization circuit can equally

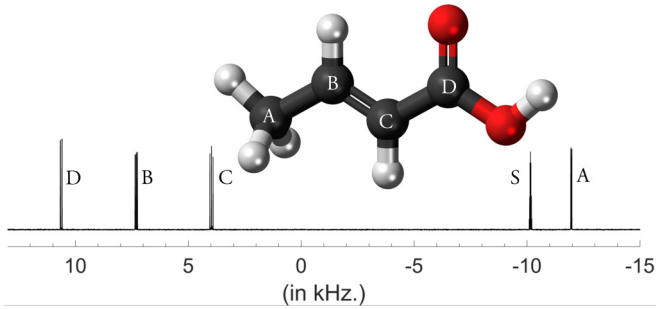


FIG. 2. The molecular structure and NMR spectrum for ^{13}C labeled crotonic acid with ^1H decoupling. The multiplet labeled S comes from the solvent, deuterated acetone; the second solvent peak at around 16.4 kHz lies outside the spectral range plotted here. As in all NMR spectra the scale of the vertical axis is arbitrary and frequencies are measured from the RF transmitter frequency with frequency increasing from right to left. For more details see Appendix A.

well be viewed as a process that randomizes the pure qubits or polarizes the mixed qubits.

A. The NMR system

Our experiment to simulate a quantum homogenizer was performed on a four-qubit liquid-state NMR quantum processor, given by the four ^{13}C nuclei in a sample of fully ^{13}C labeled crotonic acid dissolved in deuterated acetone [26,27], as described in Appendix A. The Hamiltonian parameters obtained on a 600 MHz (^1H frequency) Varian Unity Inova spectrometer at 300 K are listed in Appendix A and are the same as given in [28]. This four-qubit quantum processor can be approximated by a linear chain with strong nearest-neighbour couplings (between 42 and 72 Hz) and weak long-range couplings (no more than 7 Hz). A ^{13}C NMR spectrum of the thermal equilibrium state with ^1H decoupling is shown in Fig. 2. The multiplet labeled S comes from the solvent, and so can be ignored.

B. Initialization

NMR experiments [29] are performed on macroscopic ensembles in high temperature thermal states. For this four-spin homonuclear system, the thermal equilibrium state can be approximated as

$$\rho_{\text{th}} \approx \frac{\mathbb{1}}{16} + p(A_z + B_z + C_z + D_z), \quad (7)$$

where $p \sim 10^{-6}$ is the thermal population difference and $A_z = (\sigma_z/2) \otimes \mathbb{1} \otimes \mathbb{1} \otimes \mathbb{1}$ corresponds to the z spin state of spin A, and similarly for the other three terms. The first term, which is the four-spin maximally mixed state, is not visible in NMR experiments, and the population difference simply determines the signal strength, so it is common to describe this state using just the *deviation density matrix* [30,31], which is $A_z + B_z + C_z + D_z$.

As the thermal state is highly mixed NMR quantum information processing experiments normally begin with the preparation of a *pseudopure* state [19,20], or *effective-pure* state [21,22], whose deviation density matrix corresponds to the desired pure state. Placing spins A and B in the pseudopure

state $|00\rangle$ and spins C and D in the maximally mixed state corresponds to the deviation density matrix $A_z + B_z + 2A_zB_z$ [31], but, as discussed below, only the first two terms give any visible signal in our experiments and so it suffices to use the simpler state $A_z + B_z$. This is trivial to prepare from the thermal state by applying 90° excitation pulses to spins C and D followed by a crush gradient [31].

C. Homogenization

The homogenizer circuit was implemented using gradient-ascent pulse engineering (GRAPE) [32], which assembles a single shaped pulse from a large number of short segments, each of which is individually controlled. We designed GRAPE pulses to implement each logic gate in Fig. 1, except that when two SWAP gates are written vertically above one another a single GRAPE pulse was used to implement both gates together. Separate pulses were prepared for ten different partial swap gates, varying η in 10° steps between 0 (an identity gate, for which the simplest implementation is just to omit the gate entirely) and 90° , corresponding to a full SWAP.

Although we have described our NMR spin system as a four-qubit device, the molecule also contains spin-1/2 ^1H nuclei, which are coupled to the four ^{13}C nuclei we use as qubits. (The ^{16}O nuclei are spin-0, and so can be safely ignored.) The conventional approach to this problem is to use continuous ^1H decoupling [29] throughout the pulse sequence, but we were unable to obtain good results with this method as the length of the pulses limited the radio frequency (RF) power that could be used. Instead we repeated the approach used previously in this system in which we avoid decoupling during the pulse sequence, but designed each GRAPE pulse to tolerate couplings to ^1H nuclei [28] by averaging their fidelity over the variation in the ^{13}C Hamiltonian which arises from such coupling terms, as described in Appendix B. Pulses were also designed to tolerate some RF inhomogeneity by averaging their performance over a range of RF amplitudes.

When designing GRAPE pulses in NMR it is frequently necessary to add amplitude penalties to the function being optimized to prevent the algorithm from finding solutions with unfeasibly high RF powers. We adopted a simpler approach, using a single pre-determined amplitude for each pulse and varying only the RF phase between individual segments. In addition to sidestepping the need for amplitude limits this simplifies the underlying search, but at the cost of requiring that the individual segments are quite short, so that the effective rotation induced by each segment is small. Moreover, this approach to GRAPE avoids the computationally expensive operation of matrix exponentiation, leading to enormous speed-ups over conventional approaches. As a result this approach, when combined with the sub-system GRAPE approach described in Ref. [33], could lead to efficient scalable control. Further details of this approach can be found in Appendix C.

D. Readout

The circuit in Fig. 1 assumes conventional projective measurements in the computational basis, so that it is necessary to repeat the experiment many times to estimate f , the z

component of the Bloch vector describing each qubit. Here the ensemble nature of NMR comes into its own, as NMR spectra directly reveal the desired expectation value.

Direct observation of the NMR signal, known as the free induction decay [29], reveals the expectation value of the x and y components of the Bloch vector. To observe the z component we first apply a crush gradient, dephasing any pre-existing xy components, and then apply a 90° pulse to excite all four spins. The integrated signal intensity of each of the four multiplets seen in Fig. 2 is then proportional to f . Note that integrating to find the total signal in each multiplet is equivalent to performing a partial trace over the other spins [34].

Because we are integrating each multiplet it is not necessary to apply ^1H decoupling even during readout. However it is desirable to do so, as this reduces the width of each multiplet and so reduces the effects of noise in the integrated signal. To obtain accurate integrals it is important to process the data carefully, paying attention to phasing and baseline correction [35]. As NMR signal intensities are only *proportional* to the desired z component it is essential to obtain a suitable reference intensity against which all other intensities can be normalized. In the results below, we use two different choices of normalization, which emphasize different features of the experimental results. The use of normalized intensities means that experimental errors can take measured values of f slightly outside the theoretical limits of ± 1 , and such apparently unphysical values should not cause concern.

III. RESULTS

The experimental results are shown in Fig. 3, with the two subfigures corresponding to the two different normalization choices. In each case, the lines show the expected polarizations for each of the four qubits calculated as described in the previous section, while data points show the measured polarizations on the corresponding spins. Each experiment was repeated ten times, with the error bars showing the standard deviation around the mean.

The upper panel shows the results of normalising each intensity with respect to the average intensity of the A and B multiplets in the initial state. The experimental signal intensity is systematically lower than expected, with almost all data-points lying below the theoretical lines. The agreement for spins A and B is generally better than for spins C and D, although in all cases agreement is best close to $f = 0$.

This general pattern of signal loss is easily explained as arising from the inevitable errors in any experimental implementation. Decoherence will normally lead to signal loss, and so will coherent errors which become effectively incoherent when averaged over the experimental ensemble, for example, over different RF powers in different parts of the sample. Finally the readout process, including the initial crush gradient and the implicit partial trace, itself removes all terms in the density matrix other than single spin z magnetization. Thus errors of any kind can *only* appear as a change in the measured values of f , usually reducing these towards zero.

The experimental asymmetry observed between the erasure of pure spins A and B and the polarization of initially mixed

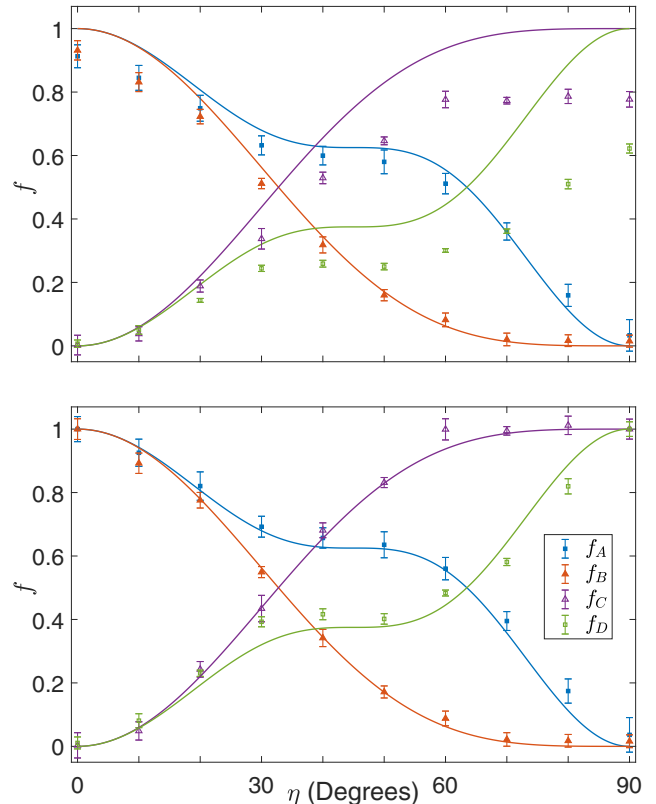


FIG. 3. Experimental results and theoretical predictions for the quantum homogenizer. Data points show the results from ten repetitions of the experiment, while solid lines show theoretical calculations using Eqs. (3)–(6). For the upper panel, signal strengths were normalized against the average intensity from spins A and B in the initial state $A_z + B_z$, while in the lower panel, the signal from each spin is normalized against a reference signal chosen for that spin.

spins C and D, in comparison with the symmetry of the theoretical predictions, is also easily understood. For spins A and B, the signal loss acts in the same direction as the quantum homogenizer process, but for spins C and D it acts against the desired process, making the effects easier to see.

The lower panel shows the results when each spin was individually normalized against its intensity in the $\eta = 0$ spectrum (for spins A and B) or $\eta = 90^\circ$ spectrum (for spins C and D). This removes the effects of signal loss during the SWAP gates, and for C and D also removes losses due to partial swap gates. The experimental data-points now lie much closer to the theoretical predictions and the expected symmetry is largely restored.

IV. INTERPRETATIONS

The experimental data show the convergence of the system qubit to the state of the reservoir qubits. This has been tested for the limiting cases of transforming a qubit from a mixed state to a pure state and from a pure to a mixed state, demonstrating that the homogenization is effective regardless of the initial states of the system or reservoir qubits. After accounting for the bias towards mixed states caused by decoherence, the experimental results are consistent with the theoretical

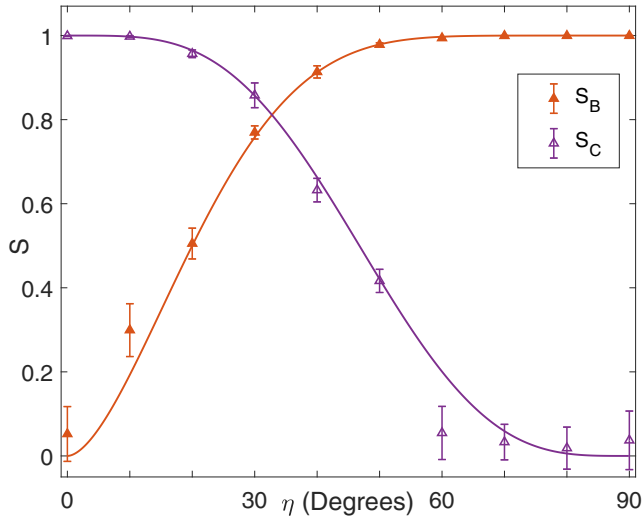


FIG. 4. Von Neumann entropies of qubits B and C against coupling strength, calculated from the experimental results and plotted against the theoretical predictions.

symmetry in the evolution of how the states evolve, where the states for the pure-to-mixed homogenization vary inversely compared to the states for the mixed-to-pure homogenization.

Pure state preparation. Figure 4 plots the von Neumann entropy

$$S = -\left(\frac{1+f}{2}\right) \log_2 \left(\frac{1+f}{2}\right) - \left(\frac{1-f}{2}\right) \log_2 \left(\frac{1-f}{2}\right) \quad (8)$$

of the theoretical and experimental qubit states against coupling strength, where f was defined in Eq. (3). Theoretical curves were calculated using Eq. (5) for f_B and $f_C = 1 - f_B$. The qubit B is the system qubit for the pure-to-mixed homogenization, while C is the system qubit for the mixed-to-pure homogenization. As expected, the qubit being transformed from a mixed to a pure state decreases in entropy, with the effect being strongest for strong coupling, while the qubit being transformed from a pure to a mixed state increases in entropy. Since all the interactions are unitary, the total von Neumann entropy of the combined homogenizer and system must remain constant. Hence it can be deduced that the entropy decrease of the mixed-to-pure system qubit C must be accompanied by an increase in the entropy of the homogenizer (qubits A and B), which is the irreducible entropic cost associated with preparing a pure state.

Scrambling. The initial pure or mixed state of a system qubit becomes indistinguishable from the original state of the homogenizer qubits, which is a special case of information scrambling. As explained in Ref. [1], the information about the system's initial state becomes hidden in mutual correlations between the homogenizer qubits. If there were no mutual correlations, one would expect the sum of the von Neumann entropies of the four qubits to equal two for all coupling strengths. The actual sum of the von Neumann entropies is in Fig. 5. While this is two for the cases of an identity or a SWAP operation, for intermediate coupling strengths it is larger. This indicates that the negative contribution to von Neumann

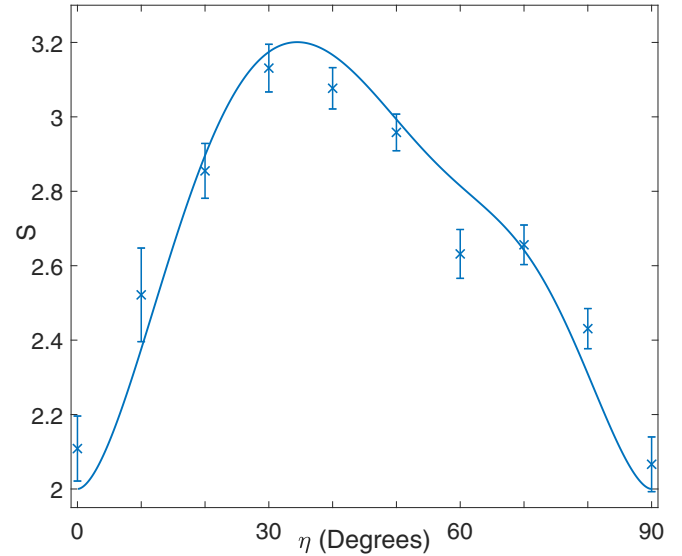


FIG. 5. Total von Neumann entropies of the four individual qubits, calculated from the experimental results and plotted against the theoretical predictions.

entropy from mutual correlations has been unaccounted for, which is due to considering only reduced density operators to describe the qubit states.

Reusability. The results in Ref. [1] show that for the regime of weak coupling and a large reservoir, the reservoir qubits remain almost unchanged by the interaction. We can therefore hypothesize that the same homogenizer could be reused for a second time (or more) to successfully homogenize more system qubits. Whilst the system we have tested here only has a small homogenizer, we can explore the hypothesis by comparing the states of the four qubits in the weak coupling regime.

Qubit A can be interpreted as interacting with a homogenizer that has already been “used” once, to homogenize B. Similarly, qubit D can be interpreted as being homogenized by a homogenizer that has already been used to homogenize C. These second system qubit states are closely aligned with the first system qubit counterparts for weak coupling, and diverge for strong coupling, in Fig. 3. This indicates that the homogenizer is minimally changed from its original state in the weak coupling regime, allowing it to perform just as effective a homogenization on the second system qubit as it did on the first. Hence, the homogenizer can be reused to some extent to give the same incremental changes in system qubit state, in the weak coupling regime. Quantifying how far the homogenizer can be reused, depending on its initial state, is a line of further theoretical and experimental work in this area, which we leave for a future paper.

V. CONCLUSIONS

We have performed an NMR demonstration of the quantum homogenizer, using the partial swap on a system of four qubits. This demonstrates the principle behind a machine that can perform processes such as information erasure and the preparation of pure states using entirely unitary interactions. The experiments show the homogenization of a pure state and

of a mixed state. The asymmetry in the evolution of the states with coupling strength can be explained by the decoherence within the experiment. After accounting for this, the results are consistent with the theoretical symmetric evolution of the pure and mixed qubit states.

Our experiment was limited to showing the principles behind a homogenization machine with a small number of NMR qubits. In theory, the quantum homogenizer can perform homogenization to arbitrarily high accuracy in the limit of an infinitely large reservoir, with vanishing deterioration to its own state in the limit of weak coupling. This is of particular interest for a number of approaches which aim to study entities that undergo no net change while enabling a transformation: resource theory [36], where such entities are called catalysts, and the theory of quantum reference frames [37], in the studies of the emergence of classicality. It is also of particular interest for the constructor theory of thermodynamics [38,39], where thermodynamic irreversibility is associated with there being tasks that can be performed to arbitrarily high accuracy in one direction, but not in the reverse. The homogenizer is therefore a candidate toy-model to demonstrate these phenomena within quantum theory.

Expanding the experimental demonstration of the homogenizer to different regimes and quantum technologies could give an additional insight into the fundamental limits to homogenizing pure and mixed states by physical machines. This may ultimately help define the limiting capabilities of quantum computation protocols, and new devices in the field of quantum thermodynamics.

ACKNOWLEDGMENTS

GB is supported by a Felix Scholarship. CM thanks the Templeton World Charity Foundation and the Eutopia Foundation for financial support. VV's research is supported by the National Research Foundation, Prime Minister's Office, Singapore, under its Competitive Research Programme (CRP Award No. NRF-CRP14-2014-02) and administered by Centre for Quantum Technologies, National University of Singapore. Quantum circuits were drawn using Quantikz [40]. This publication was made possible through the support of the ID 61466 grant from the John Templeton Foundation, as part of The Quantum Information Structure of Spacetime (QISS) Project (qiss.fr). The opinions expressed in this publication are those of the authors and do not necessarily reflect the views of the John Templeton Foundation. This research was also supported by grant number (FQXi-RFP-1812) from the Foundational Questions Institute and Fetzer Franklin Fund, a donor advised fund of Silicon Valley Community Foundation.

APPENDIX A: THE NMR SPIN SYSTEM

The NMR sample comprises a solution of fully ^{13}C labeled crotonic acid (*trans*- $\text{CH}_3\text{CH}=\text{CHCO}_2\text{H}$) dissolved in deuterated acetone and held at a temperature of 300 K. The structure is shown in Fig. 2 as a “ball and stick” diagram, with carbon atoms coloured black, hydrogen atoms white, and oxygen atoms red. As usual for liquid state NMR samples rapid molecular tumbling means that the different molecules are rendered effectively identical, and direct dipole–dipole

couplings between nuclei in different molecules are averaged out, so the system can be treated as an ensemble of identical independent copies. The deuterium signal of the solvent is used to provide a field-frequency lock, which holds the NMR transition frequencies constant.

The spin system contains ten spin-1/2 entities, four ^{13}C nuclei and six ^1H nuclei. The two ^{16}O nuclei can be completely ignored as they are spin-0, and so have no effect on the other spins. The ^1H nucleus in the hydroxyl group can also be ignored as it undergoes rapid chemical exchange [29], averaging out its interaction with other spins, leaving us with a nine spin system. This can be described by the Hamiltonian

$$\mathcal{H} = \mathcal{H}_H + \mathcal{H}_C + \mathcal{H}_{HC}, \quad (\text{A1})$$

where \mathcal{H}_H and \mathcal{H}_C comprises the chemical shifts of and homonuclear couplings [29] between the five ^1H and four ^{13}C nuclei, respectively, while \mathcal{H}_{HC} represents the heteronuclear couplings between the different nuclear types.

The RF transmitter frequency was set to 150.852078 MHz, which corresponds to zero-frequency in the NMR spectrum shown in Fig. 2. For this spectrum the \mathcal{H}_{HC} terms were removed by ^1H decoupling [29]. The frequencies in \mathcal{H}_C are given in the table below.

A	B	C	D	
−11962.2	41.6	1.5	7.1	A
	7306.0	69.6	1.2	B
		3972.1	72.3	C
			10626.1	D

Here the resonance frequencies for each spin are given down the diagonal, and couplings between spins are listed off the diagonal; all frequencies are in hertz.

APPENDIX B: ROBUST GRAPE PULSES

Of the nine relevant spin-1/2 nuclei in the spin system (see Appendix A), we only seek to perform quantum gates on the four ^{13}C nuclei, which form the system qubits, with the five ^1H nuclei providing an unwanted environment. The traditional approach is to apply a broadband decoupling sequence [29] to the ^1H environment qubits so as to average out their interactions with the system qubits. As the environment spins are not directly observed, decoupling the environment qubits is equivalent to deleting the \mathcal{H}_H and \mathcal{H}_{HC} terms from the overall Hamiltonian thereby leaving just the Hamiltonian \mathcal{H}_C , and GRAPE [32] can now be used to design quantum gates on this four-qubit system.

However, in practice it is not possible to achieve perfect ^1H decoupling, completely tracing out the environment qubits so as to allow an ideal four-qubit treatment of the system. Perfect decoupling requires extremely high RF powers, beyond realistic hardware capabilities, and will also lead to heating of the sample. Our simulations suggest that imperfect ^1H decoupling is the main source of error encountered while implementing GRAPE pulses on this system. The most direct approach to overcome this is to design a nine-qubit quantum gate that

controls both ^1H and ^{13}C excitation so as to perform an identity operation on the environment qubits, while implementing the desired four-qubit operation on system qubits. However, designing nine-qubit gates using GRAPE is computationally expensive and impractical.

Here, we adopt the approach described in Ref. [28] for designing GRAPE pulses that totally avoid environment decoupling and also have a similar computational complexity scaling to four-qubit systems. The idea is to leave the ^1H nuclei completely untouched while implementing the quantum gate, so that they can be treated as remaining in fixed eigenstates. These five spins give rise to $2^5 = 32$ possible eigenstates $\{00000, 00001, \dots, 11111\}$, but there are only 16 genuinely distinct eigenstates as the three ^1H nuclei in the methyl group are completely equivalent. By considering each of these 16 eigenstates one at a time, we obtain 16 separate system Hamiltonians. Designing a GRAPE pulse that is robust over these 16 Hamiltonians is equivalent to tracing out \mathcal{H}_H and \mathcal{H}_HC terms from the combined Hamiltonian. Therefore, at modest computational overhead, the GRAPE pulses can be made robust to the environment qubits.

APPENDIX C: PHASE-ONLY GRAPE PULSES

In GRAPE [32], the control sequence is made piecewise continuous by discretizing the total control duration T into N segments each of duration $\Delta t = T/N$. Generally, the controls for each segment j are characterized by an amplitude $\Omega(j)$ and phase $\phi(j)$ which are constant for a duration Δt . However, here we restrict the control sequence to have a fixed amplitude Ω across all N segments. In such a case, the propagator during the j th segment for a homonuclear spin system is given by

$$U_j = \exp\left(-\frac{i}{\hbar}[\mathcal{H}_0 + \Omega \cos \phi(j)I_x + \Omega \sin \phi(j)I_y]\Delta t\right), \quad (\text{C1})$$

where \mathcal{H}_0 is the internal Hamiltonian of the spin system and I_x and I_y are the total x - and y -Pauli spin-1/2 operators acting on all the spins. As described in Ref. [41], this propagator can

be expressed as a series of z and x rotations,

$$U_j = \mathcal{Z}_j \mathcal{X} \mathcal{Z}_j^\dagger, \quad (\text{C2})$$

where $\mathcal{Z}_j = \exp[-i\phi(j)I_z]$ is a diagonal matrix and $\mathcal{X} = \exp[-i(\mathcal{H}_0 + \Omega I_x)\Delta t]$ is a constant matrix, which is the same for all N segments. The operator \mathcal{X} can thus be evaluated once, and then stored for reuse, while the diagonal matrix \mathcal{Z}_j can be treated as a column vector to perform elementwise multiplication with \mathcal{X} . As a result, the evaluation of the propagator U_j can be greatly sped up, with the only computation required being elementwise multiplication of a matrix and a vector. Thus, by setting a fixed amplitude across all segments, it is possible to entirely avoid the expensive computation of matrix exponentials, while simultaneously avoiding the need for amplitude penalty functions.

Further, this construction of the propagator can greatly simplify the evaluation of gradient of the propagator with respect to the control variables, a necessary step for the GRAPE algorithm to update the controls. The only variable controls present in the propagator U_j are the phases $\phi(j)$ that appear in the diagonal matrix \mathcal{Z}_j . Since, \mathcal{Z}_j is diagonal, it is also possible to evaluate the exact result

$$d\mathcal{Z}_j/d\phi(j) = -iI_z \mathcal{Z}_j \quad (\text{C3})$$

analytically. Applying the chain rule, the exact gradient of the propagator U_j with respect to the phase ϕ_j is

$$\frac{dU_j}{d\phi(j)} = i[U_j, I_z]. \quad (\text{C4})$$

Unlike the original GRAPE algorithm [32] which relied on gradients approximated to first-order, our method can evaluate exact analytic gradients at no additional cost.

Methods for evaluating exact gradients have been discussed in Ref. [42], where evaluation of the propagators by eigendecomposition gives the exact gradients at no additional cost. However, in our method, by simply fixing the amplitudes the exact gradients can be calculated without the need of matrix exponentiation or eigendecomposition for evaluating propagators. Moreover, exact gradients are necessary [43] while using second order optimization routines like BFGS [44]. Further, the exact Hessian can also be evaluated analytically if desired, giving accelerated convergence while using Netwon–Raphson type methods [45].

-
- [1] M. Ziman, P. Stelmachovic, V. Buzek, M. Hillery, V. Scarani, and N. Gisin, Diluting quantum information: An analysis of information transfer in system-reservoir interactions, *Phys. Rev. A* **65**, 042105 (2002).
- [2] V. Scarani, M. Ziman, P. Stelmachovic, N. Gisin, and V. Buzek, Thermalizing Quantum Machines: Dissipation and Entanglement, *Phys. Rev. Lett.* **88**, 097905 (2002).
- [3] C. H. Bennett, The thermodynamics of computation—a review, *Int. J. Theor. Phys.* **21**, 905 (1982).
- [4] V. Zhirnov, R. Cavin, J. Hutchby, and G. Bourianoff, Limits to binary logic switch scaling - a gedanken model, *Proc. IEEE* **91**, 1934 (2003).

- [5] J. Hong, B. Lambson, S. Dhuey, and J. Bokor, Experimental test of Landauer’s principle in single-bit operations on nanomagnetic memory bits, *Sci. Adv.* **2**, e1501492 (2016).
- [6] A. Bérut, A. Arakelyan, A. Petrosyan, S. Ciliberto, R. Dillenschneider, and E. Lutz, Experimental verification of Landauer’s principle linking information and thermodynamics, *Nature* **483**, 187 (2012).
- [7] J. P. S. Peterson, R. S. Sarthour, A. M. Souza, I. S. Oliveira, J. Goold, K. Modi, D. O. Soares-Pinto, and L. C. Céleri, Experimental demonstration of information to energy conversion in a quantum system at the Landauer limit, *Proc. R. Soc. A* **472**, 20150813 (2016).

- [8] M. López-Suárez, I. Neri, and L. Gamaitoni, Sub- $k_B T$ microelectromechanical irreversible logic gate, *Nat. Commun.* **7**, 12068 (2016).
- [9] M. Hemmo and O. Shenker, The physics of implementing logic: Landauer's principle and the multiple-computations theorem, *Stud. Hist. Philos. Sci. B* **68**, 90 (2019).
- [10] J. Goold, M. Paternostro, and K. Modi, Nonequilibrium Quantum Landauer Principle, *Phys. Rev. Lett.* **114**, 060602 (2015).
- [11] M. H. Mohammady, M. Mohseni, and Y. Omar, Minimising the heat dissipation of quantum information erasure, *New J. Phys.* **18**, 015011 (2016).
- [12] E. P. Hanson, A. Joye, Y. Pautrat, and R. Raquépas, Landauer's principle in repeated interaction systems, *Commun. Math. Phys.* **349**, 285 (2017).
- [13] R. J. Lewis-Swan, A. Safavi-Naini, A. M. Kaufman, and A. M. Rey, Dynamics of quantum information, *Nat. Rev. Phys.* **1**, 627 (2019).
- [14] M. A. Cazalilla and M. Rigol, Focus on dynamics and thermalization in isolated quantum many-body systems, *New J. Phys.* **12**, 055006 (2010).
- [15] A. Bohrdt, C. B. Mendl, M. Endres, and M. Knap, Scrambling and thermalization in a diffusive quantum many-body system, *New J. Phys.* **19**, 063001 (2017).
- [16] P. Hayden and J. Preskill, Black holes as mirrors: quantum information in random subsystems, *J. High Energy Phys.* **09** (2007) 120.
- [17] K. A. Landsman, C. Figgatt, T. Schuster, N. M. Linke, B. Yoshida, N. Y. Yao, and C. Monroe, Verified quantum information scrambling, *Nature (London)* **567**, 61 (2019).
- [18] D. Aharonov and M. Ben-Or, Fault-Tolerant Quantum Computation with Constant Error Rate, *SIAM J. Comput.* **38**, 1207 (2008).
- [19] D. G. Cory, A. F. Fahmy, and T. F. Havel, Ensemble quantum computing by NMR spectroscopy, *Proc. Natl. Acad. Sci. USA* **94**, 1634 (1997).
- [20] D. G. Cory, M. D. Price, and T. F. Havel, Nuclear magnetic resonance spectroscopy: An experimentally accessible paradigm for quantum computing, *Physica D* **120**, 82 (1998).
- [21] N. A. Gershenfeld and I. L. Chuang, Bulk spin-resonance quantum computation, *Science* **275**, 350 (1997).
- [22] E. Knill, I. Chuang, and R. Laflamme, Effective pure states for bulk quantum computation, *Phys. Rev. A* **57**, 3348 (1998).
- [23] M. S. Anwar, D. Blazina, H. A. Carteret, S. B. Duckett, T. K. Halstead, J. A. Jones, C. M. Kozak, and R. J. K. Taylor, Preparing High Purity Initial States for Nuclear Magnetic Resonance Quantum Computing, *Phys. Rev. Lett.* **93**, 040501 (2004).
- [24] M. S. Anwar, D. Blazina, H. A. Carteret, S. B. Duckett, and J. A. Jones, Implementing Grover's quantum search on a parahydrogen based pure state NMR quantum computer, *Chem. Phys. Lett.* **400**, 94 (2004).
- [25] M. S. Anwar, J. A. Jones, D. Blazina, S. B. Duckett, and H. A. Carteret, Implementation of NMR quantum computation with parahydrogen-derived high-purity quantum states, *Phys. Rev. A* **70**, 032324 (2004).
- [26] N. Boulant, E. M. Fortunato, M. A. Pravia, G. Teklemariam, D. G. Cory, and T. F. Havel, Entanglement transfer experiment in NMR quantum information processing, *Phys. Rev. A* **65**, 024302 (2002).
- [27] K. Li, Y. Li, M. Han, S. Lu, J. Zhou, D. Ruan, G. Long, Y. Wan, D. Lu, B. Zeng, and R. Laflamme, Quantum spacetime on a quantum simulator, *Commun. Phys.* **2**, 122 (2019).
- [28] G. Bhole, J. A. Jones, C. Marletto, and V. Vedral, Witnesses of non-classicality for simulated hybrid quantum systems, *J. Phys. Commun.* **4**, 025013 (2020).
- [29] R. R. Ernst, G. Bodenhausen, and A. Wokaun, *Principles of Nuclear Magnetic Resonance in One and Two Dimensions* (Oxford University Press, Oxford, 1987).
- [30] I. L. Chuang, N. Gershenfeld, M. G. Kubinec, and D. W. Leung, Bulk quantum computation with nuclear magnetic resonance: Theory and experiment, *Proc. Roy. Soc. Lond. A* **454**, 447 (1998).
- [31] J. A. Jones, Quantum computing with NMR, *Prog. NMR Spectrosc.* **59**, 91 (2011).
- [32] N. Khaneja, T. Reiss, C. Kehlet, T. Schulte-Herbrüggen, and S. J. Glaser, Optimal control of coupled spin dynamics: design of NMR pulse sequences by gradient ascent algorithms, *J. Magn. Reson.* **172**, 296 (2005).
- [33] C. A. Ryan, C. Negrevergne, M. Laforest, E. Knill, and R. Laflamme, Liquid-state nuclear magnetic resonance as a testbed for developing quantum control methods, *Phys. Rev. A* **78**, 012328 (2008).
- [34] H. K. Cummins, C. Jones, A. Furze, N. F. Soffe, M. Mosca, J. M. Peach, and J. A. Jones, Approximate Quantum Cloning with Nuclear Magnetic Resonance, *Phys. Rev. Lett.* **88**, 187901 (2002).
- [35] J. C. Hoch and A. S. Stern, *NMR Data Processing* (Wiley, New York, 1996).
- [36] B. Coecke, T. Fritz, and R. W. Spekkens, A mathematical theory of resources, *Inform. Comp.* **250**, 59 (2016).
- [37] S. Popescu, A. B. Sainz, A. J. Short, and A. Winter, Quantum reference frames and their applications to thermodynamics, *Philosophical Transactions of the Royal Society A* (2018).
- [38] D. Deutsch and C. Marletto, Constructor theory of information, *Proc. R. Soc. A* **471**, 20140540 (2014).
- [39] C. Marletto, Constructor theory of thermodynamics, [arXiv:1608.02625](https://arxiv.org/abs/1608.02625).
- [40] A. Kay, Tutorial on the quantikz package, [arXiv:1809.03842](https://arxiv.org/abs/1809.03842).
- [41] G. Bhole and J. A. Jones, Practical pulse engineering: Gradient ascent without matrix exponentiation, *Front. Phys.* **13**, 130312 (2018).
- [42] S. Machnes, U. Sander, S. J. Glaser, P. de Fouquières, A. Gruslys, S. Schirmer, and T. Schulte-Herbrüggen, Comparing, optimizing, and benchmarking quantum-control algorithms in a unifying programming framework, *Phys. Rev. A* **84**, 022305 (2011).
- [43] J. H. M. Jensen, F. S. Møller, J. J. Sørensen, and J. F. Sherson, Exact gradients and Hessians for quantum optimal control and applications in many-body matrix product states, [arXiv:2005.09943](https://arxiv.org/abs/2005.09943).
- [44] P. De Fouquieres, S. G. Schirmer, S. J. Glaser, and I. Kuprov, Second order gradient ascent pulse engineering, *J. Magn. Reson.* **212**, 412 (2011).
- [45] D. L. Goodwin and I. Kuprov, Modified Newton-Raphson GRAPE methods for optimal control of spin systems, *J. Chem. Phys.* **144**, 204107 (2016).